LF Ground-Wave Propagation Over Irregular Terrain

Lili Zhou, Xiaoli Xi, Jiangfan Liu, and Ningmei Yu

***Abstract*—Traditional methods used to predict the ground-wave field strength at low frequency are not applicable for terrains with serious irregularities because of the analytical approximations. In this paper, the two dimensional finite-difference time-domain (FDTD) algorithm is applied to calculate the field strength of the low frequency (LF) ground wave propagating over irregular terrains. The propagation characteristics are studied as functions of the mountain's gradient, height, and width, respectively. We also focus on studying the cases with multiple mountains in the path. Moreover, the error of the traditional integral equation method is analyzed by comparisons. The results show that when the mountain's gradient and height are high, additional oscillations in the field strength will appear in front of and in the mountain region due to the wave reflection and scattering. At last, measurements of the Loran-C signals are taken along a real path between Pucheng and Tongchuan in Shaanxi province, China. It is found that most of the measured and FDTD results have good agreements while some still have big errors owing to the model approximation. The FDTD method gets better precision than the integral equation method in the irregular terrain.**

***Index Terms*—Finite-difference time-domain (FDTD) methods, ground-wave propagation, irregular terrain, low frequency.**

I. Introduction

LOW frequency ground wave has been widely used in navigation, positioning, timing and frequency dissemination systems. However, since the signals propagate over paths of varying conductivity, topography and atmosphere refraction index, it is difficult to predict them precisely, which may lead to low positioning or timing precision. In order to obtain high accuracy, it is essential to learn the characteristics of the ground wave, especially when propagating over irregular terrains [1], [2].

The investigation of LF ground-wave propagation can be traced back to the beginning of last century. The early contributions of Zenneck and Sommerfeld [3], [4] were based on a flat-earth model, where the earth surface was assumed to be a flat plane with permittivity and finite conductivity. Other pioneers such as Fock, Millington, Wait, Hufford *et al.*, further studied the spherical smooth-earth model, stratified-ground model, mixed-path model and irregular-earth model [5], [6]. For irregular terrains, two theoretical methods are usually used to predict the ground-wave propagation, namely, the Millington algorithm [7] and the integral equation method [8]. The Millington method approximates the topographic effect using an equivalent conductivity. It is simple, but the calculation error is big in the mountain region. The integral equation method considers the real topographic effect, but the accuracy is also poor when the parameters and topography change greatly along or around the paths [8]. As only a limited number of highly idealized ground-wave propagation problems have mathematically exact solutions, semianalytical/numerical and pure numerical simulation methods are appropriate ways to handle realistic ground-wave propagation problems [9]. Recently, the numerical methods including the finite element method (FEM), method of moment (MoM), finite-difference time-domain (FDTD) and parabolic-equation (PE) methods, are often applied in the research of wave propagation along the Earth's surface [9]–[20]. Former researches were more concerned in predicting the transmission losses of ground-wave in MF/HF bands or calculating the VLF-LF propagation in the Earth-Ionosphere waveguide without considering the terrain impacts. In fact, in LF band, terrain impacts are not negligible when the terrain relief is close to the wavelength. In this paper, a two-dimensional cylindrical coordinate FDTD algorithm is used to simulate the LF ground-wave propagation. The purpose is to analyze the terrain effects on the wave propagation characteristics and give the variation trends of the ground wave propagating over the paths with extremely serious irregularities. Comparing the results to those of the traditional integral equation method, the error and applicable conditions of the integral equation method is analyzed.

II. Computational Model and Lagorithms

For a flat and homogenous path, ground-wave propagation problems can be solved analytically by the flat-earth formula in a cylindrical coordinate system, detailed equations can be found in [21], it is also listed in the Appendix A for the convenience of the reader. For more complicated propagation path with varying terrain and electrical parameters, the integral equation method can be applied. The electrical field strength can be expressed as a function of the ground wave attenuation factor W [8], [22], as given by

$$E_z = \frac{\mathrm{i}120\pi I \mathrm{d}l}{\lambda a\sqrt{\theta \sin\theta}} \mathrm{e}^{\mathrm{i}ka\theta} W. \tag{1}$$

Detailed equation for W can be found in the Appendix B. The above two methods are used in the following sections as references. We now focus on the numeric method, i.e., the FDTD method, for the sake of being able to capture the real topographic effects.

The FDTD method has been well documented in the literature [23] therefore details are omitted in this paper. In the

Manuscript received May 29, 2010; revised September 04, 2010; accepted September 28, 2010. Date of publication January 31, 2011; date of current version April 06, 2011. This work was supported in part by the National Natural Science Foundation of China (No. 60671035) and in part by Shaanxi Provincial Project of Special Foundation of Key Disciplines.

L. Zhou, X. Xi, and N. Yu are with the Electrical Engineering Department, Xi'an University of Technology, Xi'an 710048, China (e-mail: cimeiyuer@126.com; xixiaoli@xaut.edu.cn; xixiaoli86@gmail.com; yuningmei@xaut.edu.cn).

J. Liu is with the Electrical Engineering Department, Northwestern Polytechnical University, Xi'an 710072, China (e-mail: liujiangfan123@163.com).

Digital Object Identifier 10.1109/TAP.2011.2109693

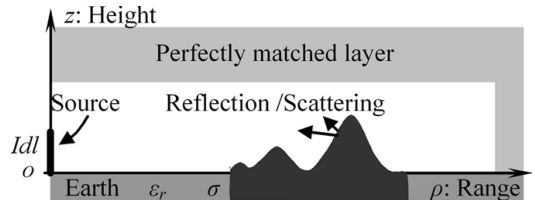

Fig. 1. Computational model.

FDTD simulation, the perfectly matched layer (PML) absorbing boundary condition (ABC) [24], [25] is very important for terminating the simulation domain without generating fake reflections. Implementation of the PML can be done by mapping the Maxwell's equations onto a stretched-coordinate-system and including lossy factors. In the cylindrical coordinate system, the coordinate stretching is defined by

$$\tilde{\rho} = \rho_L + \int_{\rho_L}^{\rho} s_\rho(\rho')\,\mathrm{d}\rho' \tag{2}$$

$$\tilde{z} = z_L + \int_{z_L}^{z} s_z(z')\,\mathrm{d}z' \tag{3}$$

where $s_\rho = k_\rho + \sigma_\rho/\mathrm{i}\omega\varepsilon_0$, $s_z = k_z + \sigma_z/\mathrm{i}\omega\varepsilon_0$ are the PML parameters. Outside PML, $s_\rho = s_z = 1$. For a lossy material as the earth, the Maxwell's equation in the PML can be described in the cylindrical coordinate system as

$$\nabla \times \overrightarrow{E} = -\mathrm{i}\omega\mu_0\bar{\bar{\mu}}\overrightarrow{H} \tag{4}$$

$$\nabla \times \overrightarrow{H} = \mathrm{i}\omega\varepsilon_0\left(\varepsilon_r + \frac{\sigma}{j\omega}\right)\bar{\bar{\varepsilon}}\overrightarrow{E} \tag{5}$$

where ε_r and σ are relative permittivity and conductivity of the earth and

$$\bar{\bar{\varepsilon}} = \bar{\bar{\mu}} = \begin{bmatrix} \frac{s_z\tilde{\rho}}{s_r\rho} & 0 & 0 \\ 0 & \frac{s_z s_r \rho}{s_r\tilde{\rho}} & 0 \\ 0 & 0 & \frac{s_r\tilde{\rho}}{s_z\rho} \end{bmatrix}. \tag{6}$$

Following the standard finite-difference approach, the field update equations can be derived.

Assuming the terrain being consistent in φ direction, the ground-wave propagation problem can be solved in a 2-D cylindrical coordinate system using the FDTD method. Fig. 1 shows the FDTD computational model.

The computational domain is defined with the size in ρ and z directions of 100 and 5.625 km, respectively. An electric dipole is located at coordinate zero. The spatial steps along ρ direction (denoted as $\Delta\rho$) and z direction (Δz) are both 18.75 m. The time step Δt is set to be 31.25 ns according to the Courant stability limit. The computational domain is meshed by $N_\rho \times N_z = 5333 \times 300$ cells with 10 cells of PML on the right and top. The left boundary is an axisymmetric boundary and a lossy ground termination is used at the bottom. The dipole source and receivers are located at one cell above the ground.

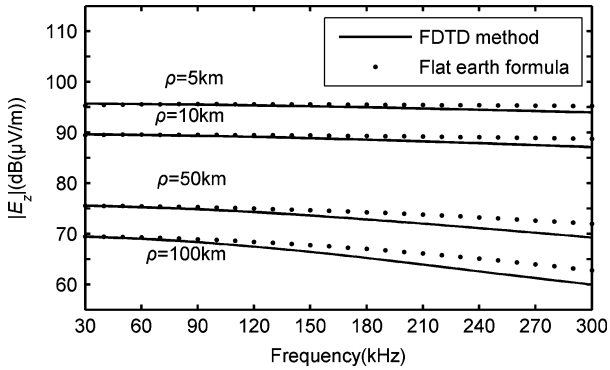

Fig. 2. Comparison of FDTD and theoretical results, E_z as a function of frequencies.

III. Simulation and Result Analysis

Algorithm Verification

Fig. 2 shows a comparison of the FDTD and flat earth formula results. The source I is a Gaussian pulse, given by

$$I = -\cos(2\pi \cdot 1.6 \times 10^5 t)\mathrm{e}^{-(1.6\times10^5 t - 2.25)^2}. \tag{7}$$

The field strength E_z is calculated as a function of frequency. The receivers are placed at $\rho = 5$, 10, 50, and 100 km, respectively. Parameters of the earth are given by $\varepsilon_r = 13$, $\sigma = 3 \times 10^{-3}$ S/m.

As shown in Fig. 2, the results of the two methods agree well at low frequency range. Due to numerical dispersion, larger deviation is observed at higher frequency and longer propagation distance. Better accuracy can be achieved using smaller grid cell size.

A. A Single Mountain in the Propagation Path

Using the FDTD method, the ground-wave propagation characteristics over a single mountain with Gaussian shape are studied. The terrain function of the Gaussian-shaped mountain is given by

$$z(\rho) = H\mathrm{e}^{-9(\rho-\rho_0/l)^2} \tag{8}$$

where ρ is the distance, l is a parameter for controlling the mountain width, H is the height, and ρ_0 is the distance form the antenna to the center of the mountain. An average slope factor $\bar{\beta}$ is used to express the steepness of a mountain, given by

$$\bar{\beta} = \frac{2}{L_s}\int_{\rho=\rho_0-L_s/2}^{\rho=\rho_0} \arctan(z'(\rho))\mathrm{d}\rho\frac{180}{\pi} \tag{9}$$

where L_s is the real width of a mountain and $L_s \approx 1.25l$.

Fig. 3(a) shows the electric field strength at 100 kHz over a Gaussian mountain with a fixed width but different heights. The result from the flat earth model is taken as reference. The parameters used in the simulation are given as follows: $l = 8$ km; $L_s = 10$ km; $\rho_0 = 50$ km; $H = 0.25$ km, 0.5 km, 0.75 km, 1

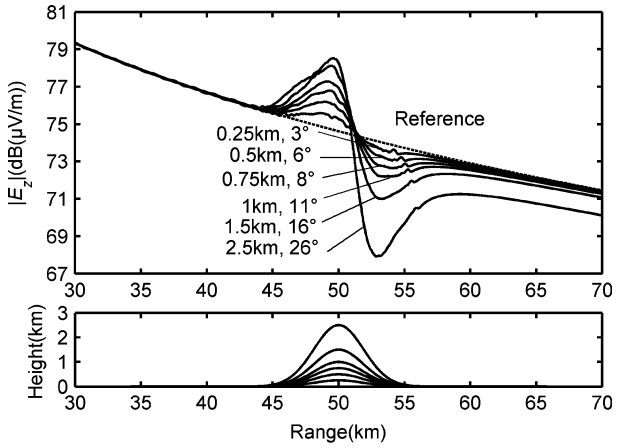

(a)

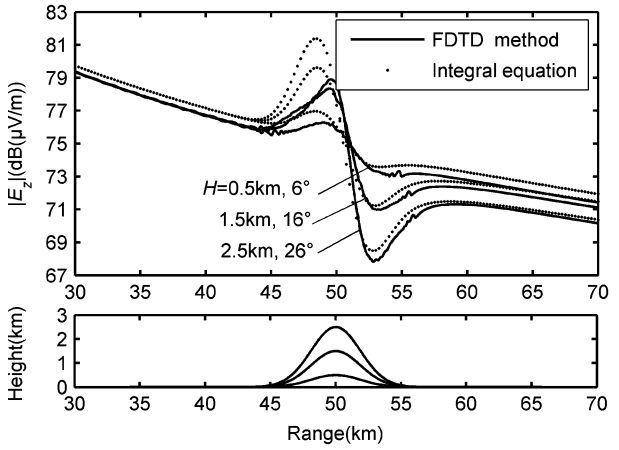

(b)

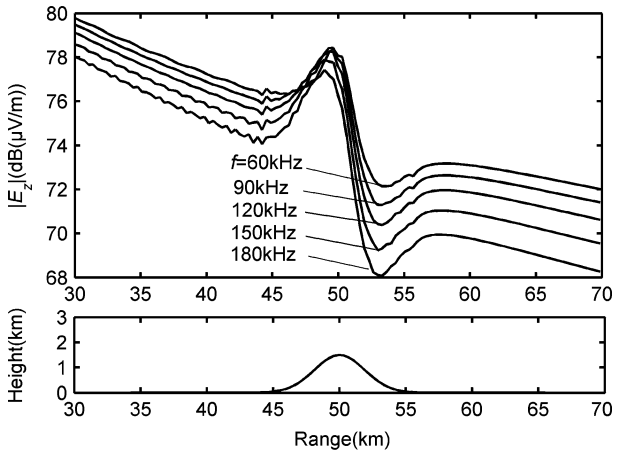

(c)

Fig. 3. Filed strength distribution over the propagation paths with a Gaussian-shaped mountain of the same width but different heights: (a) $|E_z|$ at $f = 100\,\mathrm{kHz}$ calculated by FDTD method. (b) Comparison of $|E_z|$ between FDTD and integral equation results. (c) $|E_z|$ distribution at different frequencies ($\bar{\beta} = 16°$).

km, 1.5 km, and 2.5 km leading to an average slope of 3°, 6°, 8°, 11°, 16°, and 26°, respectively.

The integral equation method is the only theoretical method which is capable of taking the terrain effects into account. In order to study the applicable conditions of the integral equation method, its results are compared to the FDTD ones, shown in Fig. 3(b). We may note that the integral equation results are calculated in a 2-D Cartesian coordinate system, which represents a uniform terrain in the perpendicular direction. This is acceptable when the distance between the mountain and transmission antenna is sufficiently far. Fig. 3(c) shows the electric field strength at different frequencies over a mountain with $H = 1.5\,\mathrm{km}$, corresponding to an average slope of 16°. The frequencies are 60, 90, 120, 150, and 180 kHz, respectively.

As shown in Fig. 3(a), the flat-earth model gives a good prediction before the mountain. In the mountain region, the amplitude of the electric field $|E_z|$ increases first while the maximum value appears when approaching the mountain top. After that, $|E_z|$ falls rapidly as the topographic height decreasing. The minimum value appears when reaching the mountain foot. In the end, the field strength increases again and the variation gradually tends to be stable at $1 \sim 3$ wavelength from the mountain. It is observed that when the mountain is lower than 1 km ($\lambda/3$), the $|E_z|$ difference between FDTD and the flat-earth model result is less than 0.2 dB. This value increases as increasing mountain height H, at $H = 2.5\,\mathrm{km}$ ($5\lambda/6$), the difference is 1.3 dB. The results in Fig. 3(b) show that when the steepness of the mountain is small, the field strength calculated by the two methods match well. In the flat areas in front and after the mountain, the difference is less than 0.6 dB. The discrepancy mainly exists in the mountain region during the terrain rising and higher mountain leads to bigger difference. This is caused by the approximation of the integral equation method, where the terrain change after the receiver position is not considered, so that the backscattered fields are neglected. As shown in Fig. 3(b), when $H = 0.5\,\mathrm{km}$, the difference is less than 1 dB; when $H = 1.5\,\mathrm{km}$, it is up to 1.5 dB; when $H = 2.5\,\mathrm{km}$, the difference increases to 4 dB. As expected, similar phenomenon is found in Fig. 3(c). At different frequencies in LF band, the higher the frequency is, the greater $|E_z|$ change is observed in the mountain region.

Fig. 4(a) shows the electric field strength $|E_z|$ at 100 kHz over a mountain with the same height but different widths. The flat earth model result is also shown as reference. The parameters used in the simulation are given as follows: $H = 1.5\,\mathrm{km}$; $\rho_0 = 50\,\mathrm{km}$; $L_s = 2.5\,\mathrm{km}$, 5 km and 15 km leading to an average slope of 49°, 30°, and 11°, respectively. Some of the results are compared in Fig. 4(b) with those from the integral equation method, too.

As shown in Fig. 4(a), steeper mountain slope leads to larger field attenuation after the mountain. When the average slope is greater than 30°, in front of the mountain there are significant oscillations stemming from the reflection and scattering effects of the mountain. Refining the FDTD mesh does not change the result, which proves that the simulation has been converged and the oscillation is not artificial. The distances between the nodal/antinodal points in the oscillation are around half wave length of the source, which also proves that the oscillation is caused by the reflection. As shown in Fig. 4(b): when the mountain is very steep, in front of the mountain, there is a big difference between the $|E_z|$ calculated by the FDTD method and the integral equation method. The integral equation method cannot catch the reflection because the terrain change after the observation point is not taken into consideration. Therefore no oscillation is observed in the integral equation results. This tells us

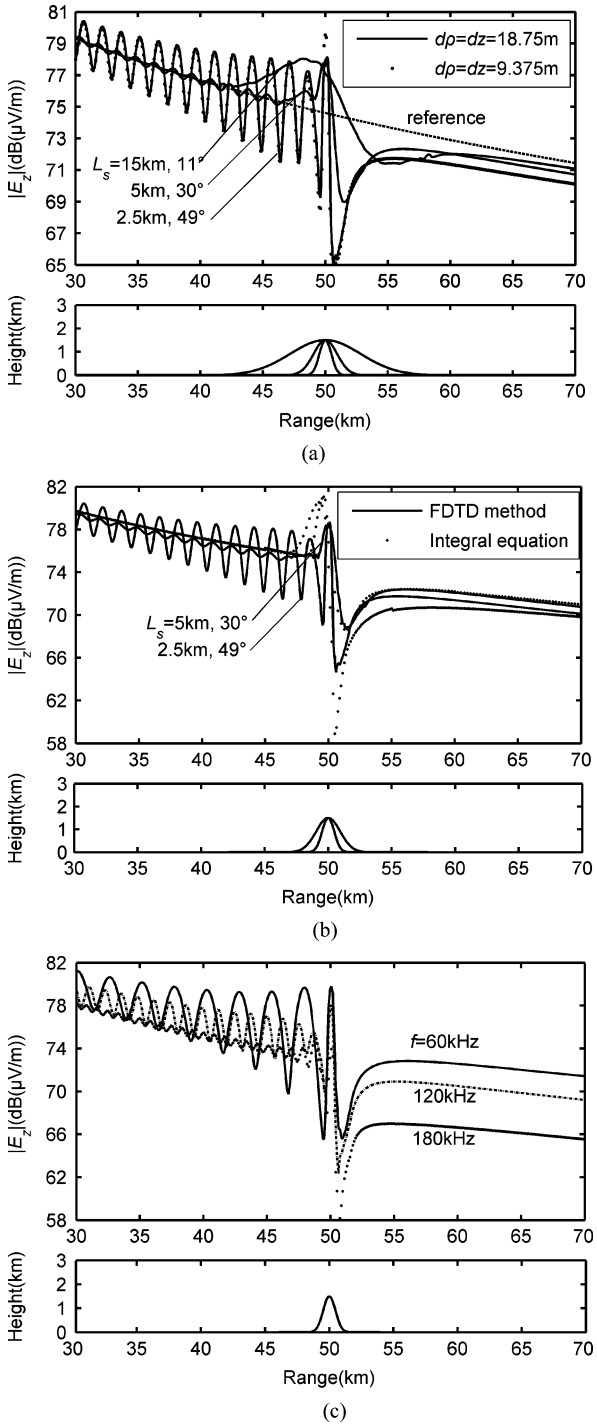

Fig. 4. Filed strength distribution over the propagation paths with a Gaussian-shaped mountain of the same height but different widths: (a) $|E_z|$ at $f = 100\,\mathrm{kHz}$ calculated by FDTD method. (b) Comparison of $|E_z|$ between FDTD and integral equation results. (c) $|E_z|$ distribution at different frequencies ($\bar{\beta} = 49°$).

that when the topographical slope is extremely high, the accuracy of the integral equation method is so low that the method is no longer applicable.

Fig. 4(c) shows the $|E_z|$ field at different frequencies, i.e., 60, 120, and 180 kHz, over a mountain with $L_s = 2.5$ km, $\bar{\beta} = 49°$. Similar propagation/reflection effects are observed in the FDTD results, which cannot be predicted by the integral equation method. It is also noted that at lower frequency, the attenuation after the mountain is smaller, while the oscillation amplitude in front of the mountain is larger.

B. Multiple Mountains in the Propagation Path

In order to study the effects on the ground wave propagation over multiple mountains, several 100-km-long propagation paths with two or three mountains of different center distances are taken as examples. The mountain is 1.5 km high, 10 km wide ($\bar{\beta} = 16°$) and the center distances d_s are 5 km, 10 km and 30 km respectively. The $|E_z|$ results calculated by the FDTD method and the integral method are shown in Fig. 5(a)–(f). It is noted that, when there are multiple mountains with the same shape in the propagation path and the mountains do not overlap with each other, the characteristics of ground wave propagation over each mountain is basically the same. After certain distance (for example, 80 km), all the results are more or less identical. In addition, the results of two methods agree well and the calculation error mainly exists in the mountain region during the terrain rising. However, if the mountains overlap with each other, oscillation is observed in the hollow or in front of the mountains, caused by (multiple) wave reflection/scattering. This oscillation cannot be predicted by the integral equation method.

C. Comparison Between FDTD and Measurement Results

The field strength along a path between Pucheng (a Loran-C station) and Tongchuan is measured by a Locus 1030 receiver and it is calibrated by the data of Lintong monitoring station. The latitude and longitude are measured by a THC-1 GPS receiver. The transmitting power of Pucheng station is $1800\,\mathrm{kw} \pm 100\,\mathrm{kw}$. The geographic information is obtained from a digital geographic information system. Among all the measured data, points 1 to 8 are located approximately along one propagation path. Fig. 6 shows the topography of experimental region and the distribution of measurement points. The field strength calculated by the FDTD method and the measured results are compared in Fig. 7.

It can be seen that the tendency of FDTD result is consistent with the reference result obtained by the flat earth model. A long propagation path with overlapping mountains leads to $|E_z|$ oscillations at unequal amplitude as the terrain varies. The oscillation has a wavelength of half of the source's wavelength and it is significant in the region with large terrain gradient. As shown in Fig. 7, the largest error between the FDTD result and the measurement happens at point 4 and 8, where the terrain changes dramatically in the cross sectional plane perpendicular to the propagation path. This tells us that the error is mainly due to the neglected 3-D topography changes.

IV. Conclusion

In this paper, a 2-D FDTD method is applied to calculate the electric field strength of LF ground wave propagating over irregular terrains. The propagation characteristics are investigated as functions of the mountain's height, width and gradient. The cases with multiple mountains in a propagation path are also analyzed. The FDTD and measurement results show that when the gradient of the mountain is high, half-wavelength oscillations appear before or between the mountain regions. This is due to

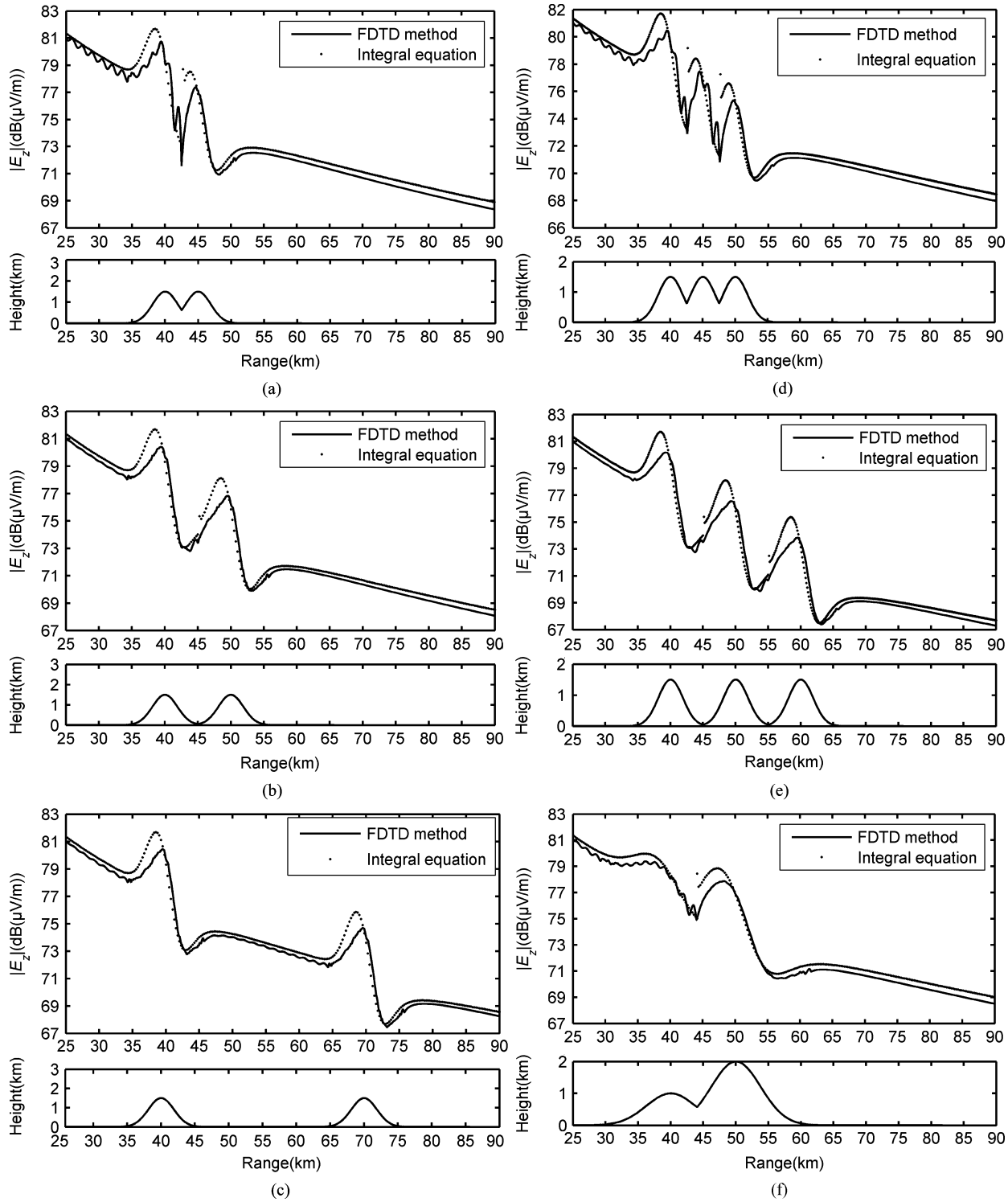

Fig. 5. Filed strength distribution over the propagation paths with multiple mountains of different center distances: (a) $|E_z|$ at 100 kHz, $d_s = 5$ km, double mountains along propagation path, (b) $|E_z|$ at 100 kHz, $d_s = 10$ km, double mountains along propagation path, (c) $|E_z|$ at 100 kHz, $d_s = 30$ km, double mountains along propagation path, (d) $|E_z|$ at 100 kHz, $d_s = 5$ km, three mountains along propagation path, (e) $|E_z|$ at 100 kHz, $d_s = 10$ km, three mountains along propagation path (f) $|E_z|$ at 100 kHz, double different shape mountains along propagation path.

the wave reflection and scattering, the higher the gradient (or lower frequency) is, the greater the oscillations are. These oscillations cannot be captured by the integral equation method, although it is the only theoretical method being able to take the terrain effect into account. Therefore, numerical method is the only candidate for calculating ground wave propagation over irregular terrain with significant topographic change. The utilization of a 2-D cylindrical coordinate FDTD modeling leads to errors at the points where the terrain changes dramatically in the cross sectional plane perpendicular to the propagation path. However, at most of the observation points, the FDTD results agree well with the measurement.

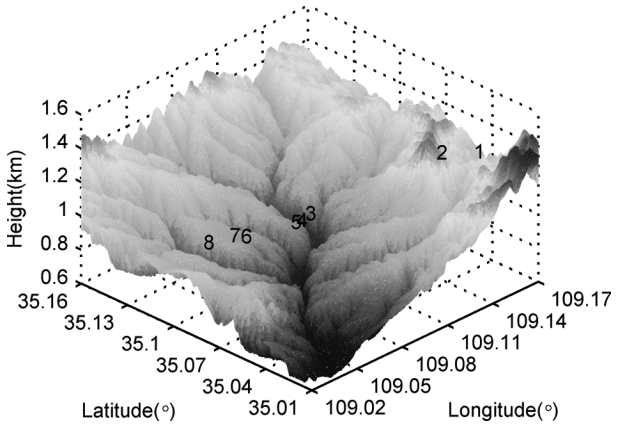

Fig. 6. Topography of the experimental region and distribution of the measured points.

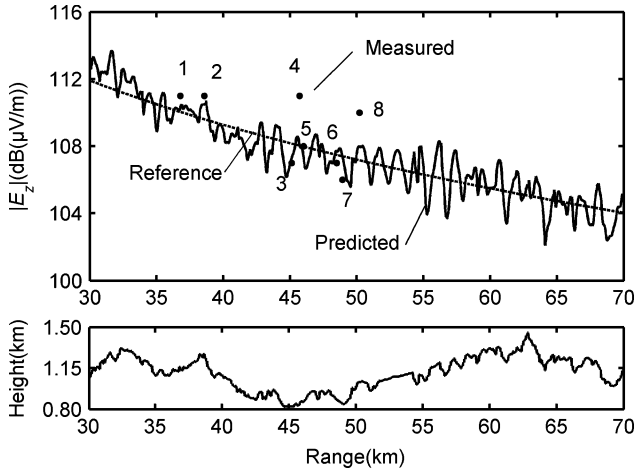

Fig. 7. Comparison of FDTD and measured results.

APPENDIX

Flat Earth Formulation: If the distance between the transmitter and receiver is short and the wave propagation path is homogenous and flat, the ground-wave field strength can be solved by the flat-earth formula. In the cylindrical coordinate system, assuming the dipole source height is h from the ground, the observation height is z, the horizontal distance between the observation point and the source is ρ, the vacuum permeability is μ_0, the earth wave number k_g is much larger than the free space wave number k_0 and both of the observation point and source are not too far from the ground, then the theory expression of the vertical field strength is as follows [22]:

$$\begin{aligned} E_z = \frac{\omega\mu_0 Idl}{2\pi k_0}\Bigg\{ & \frac{\mathrm{e}^{-\mathrm{i}k_0R_1}}{2}\left[\frac{k_0}{\mathrm{i}R_1}-\frac{1}{R_1^2}+\frac{\mathrm{i}}{k_0R_1^3}\right. \\ & \left.-\left(\frac{z-h}{R_1^2}\right)^2\cdot\left(\frac{k_0}{\mathrm{i}R_1}-\frac{3}{R_1^2}+\frac{3\mathrm{i}}{k_0R_1^3}\right)\right] \\ & +\frac{\mathrm{e}^{-\mathrm{i}k_0R_2}}{2}\left[\frac{k_0}{\mathrm{i}R_2}-\frac{1}{R_2^2}+\frac{\mathrm{i}}{k_0R_2^3}\right. \\ & \left.-\left(\frac{z+h}{R_2}\right)^2\left(\frac{k_0}{\mathrm{i}R_2}-\frac{3}{R_2^2}+\frac{3\mathrm{i}}{k_0R_2^3}\right)\right] \\ & -\frac{\mathrm{e}^{-\mathrm{i}k_0R_2}k_0^3}{k_g}\sqrt{\frac{\pi}{k_0R_2}}\mathrm{e}^{\mathrm{i}P_2}F(P_2)\Bigg\} \end{aligned} \tag{A1}$$

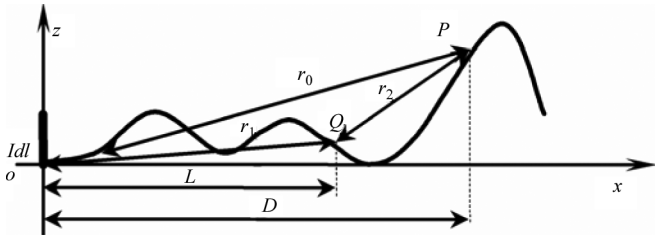

Fig. 8. Computational model.

where $R_1=\sqrt{\rho^2+(z-h)^2}$, $R_2=\sqrt{\rho^2+(z+h)^2}$

$$P_2=\frac{k_0^3R_2}{2k_g^2}\left(\frac{k_0R_2+k_g(z+h)}{k_0\rho}\right)^2 \tag{A2}$$

$$F(P_2)=\int_{P_2}^{\infty}\frac{\mathrm{e}^{-\mathrm{i}t}}{\sqrt{2\pi t}}dt. \tag{A3}$$

Integral Equation Method: The integral equation method [22] is the only theoretical method which takes the terrain effect in to consideration. For a simulation model shown in Fig. 8, the electric field strength E_z can be expressed as

$$E_z=\frac{\mathrm{i}120\pi Idl}{\lambda a\sqrt{\theta\sin\theta}}\mathrm{e}^{\mathrm{i}ka\theta}W \tag{B1}$$

where a is the earth radius, θ is the great-circle angular distance, the dipole direction is set along the z axis and the observation point P is located at $y=0$ plane. In (B1), W is the ground wave attenuation factor, given by

$$\begin{aligned} W=1-\mathrm{e}^{-\mathrm{i}\pi/4}\frac{r_0}{x}\sqrt{\frac{k}{2\pi}}\int_0^D W(Q)\mathrm{e}^{\mathrm{i}k(r_1+r_2-r_0)} \\ \cdot\left[\Delta_g+\left(1+\frac{1}{\mathrm{i}kr_2}\right)\frac{\partial r_2}{\partial n}\right]\sqrt{\frac{D}{L(D-L)}}\mathrm{d}L. \end{aligned} \tag{B2}$$

Here, Q is the integration point along the path, r_0 denotes the distance from the source to the observation point, r_1 and r_2 denote the distances from the observation point to the source and Q, respectively. L and D represent the horizontal distances from Q to the source and P, respectively.

REFERENCES

[1] G. Johnson, R. Shalaev, R. Hartnett, P. Swaszek, and M. Narins, "Can loran meet GPS backup requirements?," *IEEE Aerosp. Electron. Syst. Mag.*, vol. 20, no. 2, pp. 3–12, Feb. 2005.

[2] D. Last and P. Williams, "New ways of looking at Loran-C ASFs," presented at the 31st Int. Loran Assoc. Convent. Tech. Symp., Wash., DC, Oct. 2002.

[3] J. Zenneck, "Propagation of plane EM waves along a plane conducting surface," *Ann. Phys.*, vol. 23, pp. 846–866, Sep. 1907.

[4] A. N. Sommerfeld, "Propagation of waves in wireless telegraphy," *Ann. Phys.*, vol. 81, pp. 1135–1153, Dec. 1926.

[5] J. R. Wait, "The ancient and modern history of EM ground-wave propagation," *IEEE Antennas Propag. Mag.*, vol. 40, no. 5, pp. 7–24, Oct. 1998.

[6] W. Y. Pan, *LF VLF ELF Wave Propagation*. Chengdu, China: UEST, 2004.

[7] N. DeMinco, "Propagation prediction techniques and antenna modeling (150 to 1705 kHz) for intelligent transportation systems (ITS) broadcast applications," *IEEE Antennas Propag. Mag.*, vol. 42, no. 4, pp. 9–33, Aug. 2000.

[8] H. Gesny and O. Ravard, "Propagation over irregular terrain in the VHF band a review of integral equation models," in *Proc. IEE Nat. Conf. Antennas Propag.*, Apr. 1, 1999, pp. 61–64.
[9] F. Akleman and L. Sevgi, "A novel MoM-and SSPE-based ground-wave-propagation field-strength prediction simulator," *IEEE Antennas Propag. Mag.*, vol. 49, no. 5, pp. 69–82, Oct. 2007.
[10] G. Apaydin and L. Sevgi, "FEM-based surface wave multimixed-path propagator and path loss predictions," *IEEE Antennas Wireless Propag. Lett.*, vol. 8, pp. 1010–1013, 2009.
[11] L. Sevgi, "Groundwave modeling and simulation strategies and path loss prediction virtual tools," *IEEE Trans. Antennas Propag.*, vol. 55, pp. 1591–1598, Jun. 2007.
[12] W. Y. Pan, H. Y. Peng, and H. Q. Zhang, "Parabolic equation algorithm of wave attenuation along inhomogeneous smooth ground," *Chin. J. Radio Sci.*, vol. 21, no. 1, pp. 37–42, Feb. 2006.
[13] L. L. Zhou, X. L. Xi, and N. M. Yu, "Comparison of three methods of calculating low frequency ground-wave propagation over irregular terrain," *Chin. J. Radio Sci.*, vol. 24, no. 6, pp. 1158–1163, Dec. 2009.
[14] S. A. Cummer, "Modeling electromagnetic propagation in the earth-ionosphere waveguide," *IEEE Trans. Antennas Propag.*, vol. 48, pp. 1420–1429, Sep. 2000.
[15] J. J. Simpson and A. Taflove, "Three-dimensional FDTD modeling of impulsive ELF propagation about the earthsphere," *IEEE Trans. Antennas Propag.*, vol. 52, pp. 443–451, Feb. 2004.
[16] J. P. Berenger, "FDTD computation of VLF-LF propagation in the earth-ionosphere waveguide," *Ann. Telecommun.*, vol. 57, no. 11–12, pp. 1059–1090, 2002.
[17] Y. Wang, H. G. Xia, and Q. S. Cao, "Analysis of ELF propagation along the earth surface using the FDTD model based on the spherical triangle meshing," *IEEE Antennas Wireless Propag. Lett.*, vol. 8, pp. 1017–1020, 2009.
[18] J. J. Simpson and A. Taflove, "A review of progress in FDTD Maxwell's equations modeling of impulsive subionospheric propagation below 300 kHz," *IEEE Trans. Antennas Propag.*, vol. 55, pp. 1582–1590, Jun. 2007.
[19] A. V. Popov and V. V. Kopeikin, "Electromagnetic pulse propagation over nonuniform earth surface: Numerical simulation," *Progr. Electromagn. Res. B*, vol. 6, pp. 37–64, 2008.
[20] G. Apaydin and L. Sevgi, "Numerical investigations of and path loss predictions for surface wave propagation over sea paths including hilly island transitions," *IEEE Trans. Antennas Propag.*, vol. 58, pp. 1302–1314, Apr. 2010.
[21] R. W. P. King and S. S. Sandler, "The electromagnetic field of a vertical electric dipole over the earth or sea," *IEEE Trans. Antennas Propag.*, vol. 42, pp. 382–389, Mar. 1994.
[22] T. S. M. Maclean and Z. Wu, *Radiowave Propagation Over Ground*. London, U.K.: Chapman and Hall, 1993.
[23] A. Taflove, *Computational Electrodynamics: The Finite-Difference Time-Domain Method*. Norwood, MA: Artech House, 2000.
[24] F. L. Teixeira and W. C. Chew, "Systematic derivation of anisotropic PML absorbing media in cylindrical and spherical coordinates," *IEEE Microw. Guided Wave Lett.*, vol. 11, pp. 371–373, Nov. 1997.
[25] L. L. Zhou, X. L. Xi, N. M. Yu, and Y. R. Pu, "Modeling of LF ground-wave propagation at short distances based on 2-D cylindrical-coordinate FDTD method," in *Proc. 8th Int. Symp. Antennas, Propag. EM Theory, ISAPE*, 2008, pp. 855–858.

Lili Zhou received the B.S. and M.S. degrees from Xi'an University of Technology, Xi'an, China, in 2004 and 2007, respectively, where she is currently working toward the Ph.D. degree.

Xiaoli Xi received the B.S. degree in applied physics from the University of Defense Technology, ChangSha, China, in 1990, the M.S. degree in biomedical engineering from the Fourth Military Medical University, Xi'an, China, in 1998, and the Ph.D. degree in electrical engineering from Xi'an Jiaotong University, Xi'an, China, in 2004.

She is currently a Professor with the Department of Electric Engineering, Xi'an University of Technology, Xi'an. Her recent research interests include wave propagation, antenna design, and communication signal processing.

Jiangfan Liu received the B.S. and M.S. degrees from Xi'an University of Technology, Xi'an, China, in 2004 and 2007, respectively. He is currently working toward the Ph.D. degree at Northwestern Polytechnical University.

Ningmei Yu received the B.S. degree in electronic engineering from Xi'an University of Technology, Xi'an, China, in 1986 and the M.S. and Ph.D. degrees in electronic engineering from Tohoku University, Sendai, Japan, in 1996 and 1999, respectively.

She is currently a Professor with the Department of Electric Engineering, Xi'an University of Technology, Xi'an.